11. Bitelli G., Ferretti A., Gianicco C. et al. Subsidence Monitoring in Emilia-Romagna Region (Italy) from 2016 to 2021: From InSAR and GNSS Integration to Data Analysis. *Remote Sensing*. 2025. Vol. 17, Iss. 6. ID 947.
12. Mullojanova G. M., Aminzhanova M. B. Concept of Monitoring of Earth Surface Displacement and Deformation by Remote Sensing Data. *Economy and Society*. 2024. Vol. 121, Iss. 6-1. pp. 1230–1233.
13. Sidiq T. P., Gumilar I., Abidin H. Z. et al. Spatial Distribution and Monitoring of Land Subsidence Using Sentinel-1 SAR Data in Java, Indonesia. *Applied Sciences*. 2025. Vol. 15, Iss. 7. ID 3732.
14. Shevchuk R. V., Manevich A. I., Akmatov D. Zh., Urmanov D. I., Shakirov A. I. Geodynamic Monitoring of the Ground Surface and Mining Industry Infrastructure Using Radar Interferometry. *Russian Mining Industry*. 2022. Vol. 5. pp. 99–104.
15. Koptyakov D. A., Masalsky N. A., Kharisov T. F., Balek A. Y. Application of Interferometry to Describe Landside Processes Associated with the Karakechinsky Deposit. *Izvestija Tulskogo Gosudarstvennogo Universiteta. Nauki o Zemle*. 2024. Vol. 3. pp. 376–387.
16. Zhai M., Liu Q., Tao Q., Liu G. SBAS InSAR Subsidence Monitoring for Mining Areas Based on Levelling Constraints. *Journal of Physics Conference Series*. 2023. Vol. 2620, Iss. 1. ID 012003.
17. Pozdnyakov A. P. Application of satellite radar interferometric synthetic aperture (InSAR) for the development of oil and gas fields. *Neftegaz*. 2023. Available at: https://neftegas.info/articles/article/73 (accessed: 28.08.2025).
18. Zhai G., Yang H., Shirzaei M., Manga M., Rumeng G. S54B-01 Mechanisms of induced seismicity associated with subsurface mining activities: insights from poroelastic modeling of fluID injection and extraction. *AGU Fall Meeting Abstracts*. 2024. Available at: https://agu.confex.com/agu/agu24/meetingapp.cgi/Paper/1664762 (accessed: 28.08.2025).
19. Osmanov R. S. Application of InSAR methods for determining deformation source parameters: Integration with classical surface monitoring techniques. *Proceedings of the Digital Reality Conference 2022*. 2022. pp. 20–26.
20. Ge L., Chang H. -C., Rizos C. Mine Subsidence Monitoring Using Multi-source Satellite SAR Images. *Photogrammetric Engineering & Remote Sensing*. 2007. Vol. 73, Iss. 3. pp. 259–266.
21. Perski Z., Nescieruk P., Wojciechowski T. How to minimize the risk of landslides for hydrotechnical structures in Poland. *Inżynier Budownictwa*. 2021. Vol. 10. pp. 34–38.
22. Yan H., Dai W., Xu W. et al. A method for correcting InSAR interferogram errors using GNSS data and the K-means algorithm. *Earth Planets Space*. 2024. Vol. 76, Iss. 51. DOI: 10.1186/s40623-024-01999-5
23. Tomás R., Diaz E., Szeibert W. T. et al. Geomorphological characterization, remote sensing monitoring, and modeling of a slow-moving landslide in Alcoy (Southern Spain). *Landslides*. 2023. Vol. 20, Iss. 6. pp. 1293–1301.
24. ECMWF ERA5 Reanalysis. Available at: https://cds.climate.copernicus.eu/ (accessed: 28.08.2025).
25. GMTSAR. Available at: https://github.com/gmtsar/gmtsar (accessed: 28.08.2025).
26. StaMPS. Available at: https://homepages.see.leeds.ac.uk/~earahoo/stamps/ (accessed: 28.08.2025).
27. LiCSAR. Available at: https://comet.nerc.ac.uk/COMET-LiCS-portal/ (accessed: 28.08.2025).
28. Industrial Zone of Kentau Declared as an Ecological Emergency Zone until 2075. Available at: https://www.zakon.kz/pravo/6477316-promyshlennaya-zona-kentau-obyavlena-zonoy-chrezvychaynoy-ekologicheskoy-situatsii-do-2075-goda.html (accessed: 28.08.2025). EM

I. A. PANTELEEV[1], *Head of Laboratory, Doctor of Physical and Mathematical Sciences*
I. S. LOMAKIN[2], *Senior Researcher, Candidate of Engineering Sciences*
A. A. BARYAKH[3], *Professor, Doctor of Engineering Sciences, Academician of the Russian Academy of Sciences, bar@Mi-Perm.ru*

[1]*Institute of Continuous Media Mechanics–Division of the Perm Federal Researcher Center, Ural Branch, Russian Academy of Science, Perm, Russia*
[2]*Mining Institute–Division of the Perm Federal Researcher Center, Ural Branch, Russian Academy of Science, Perm, Russia*
[3]*Perm Federal Researcher Center, Ural Branch, Russian Academy of Science, Perm, Russia*

INCLUSION OF SALT ROCK JOINTING IN EVALUATION OF LOAD-BEARING CAPACITY OF RIB PILLARS

The study assesses the effect of including the decrease in elastic properties of salt rocks in calculation of the bearing capacity of different-size rib pillars under varying effective pressure. Based on the review of domestic and foreign reference sources, we selected the correlation between the change in the uniaxial compression strength and the decrease in Young's modulus. A modification of the approach to estimation of loading of rib pillars is proposed. It is based on the mathematical modeling of normalized stress intensity at the central point of a pillar. In this article, this calculation model is implemented as a case-study of productive sylvinite stratum Kr II at the Verkhnekamskoe (Upper Kama) salt deposit. The approximation relationships for the decrease in elastic properties with an increase in maximum effective stress are based on the results of laboratory experiments on step-by-step uniaxial compression of sylvinite specimens. Based on the results of computational experiments, we find that the dependence of elastic properties of sylvinite on maximum principal stress has the most significant impact on the load-bearing capacity of pillars with width-to height ratios of no more than 1 at the effective pressure of total undermining. For instance, the maximum change in the degree of loading of the rib pillar is 26%, from 0.5 to 0.63, and this occurs for a pillar with a shape factor of 0.75.

Keywords: *Room-and-pillar mining system, pillar stability, Verkhnekamskoe Salt Deposit, mathematical modeling, fracturing, elastic moduli*
DOI: *10.17580/em.2025.02.07*

Introduction

One of the widespread methods of underground mining is the room-and-pillar mining system. This system provides maintenance of overlying strata by load-bearing elements of various sizes [1–4]. Mining operations are carried out at the Verkhnekamskoe (Upper Kama) salt deposit (VKSD) with some productive rocks left in the form of rib pillars supporting the overlying rock strata. The stability of the rib pillars directly relates to the safety of the water-protective layer that separates the aquifer from the mined-out space of the mine. A breach in the continuity of the water-protective layer leads to the breakthrough of fresh water into the mine workings, to intense dissolution of salt rocks and to ultimately flooding of the mine with enormous socio-economic consequences.

In accordance with current regulatory documents [5, 6], the calculation of the loading degree of rib pillars at VKSD is based on the Turner–Shevyakov method [7, 8]. According to this method, the loading degree is determined by the ratio of the load acting on a pillar to its bearing capacity. In this case, the load on a pillar is determined by the weight of rock mass above it, and the bearing capacity depends on the shape of the pillar, the strength of the rocks, and several other geological factors that are specific to the deposit:

$$C = \xi \frac{\gamma(a+b)H_0}{bk_f\sigma_m} \le [C], \quad (1)$$

when ξ is the coefficient taking into account the change in the load on the pillars due to the influence of various mining factors; γ is the specific weight, N/m^3; H_0 is the maximum distance between the ground surface and the roof of the chamber, *m*, m; *a* is the width of chambers; *b* is the width of rib pillars, m; k_f is the pillar shape coefficient; σ_m is the strength of rocks, Pa; $C, [C]$ is the calculated and permissible loading degree on the rib pillar, respectively. Engineering relation (1), in accordance with the limitations of the Turner-Shevyakov approach, can be used for relatively simple development conditions: subhorizontal occurrence of productive strata, canonical geometry of pillars, periodic regular system of their arrangement, etc. At the same time, this ratio disregards the nature of stress distribution in the pillar volume.

Using multivariate mathematical modeling methods, it has been shown in [9] that the degree of loading on the rib pillar can be calculated by determining the maximum normalized stress intensity K^*, which is achieved in each vertical section of the pillar:

$$C \approx K^*, \quad (2)$$

when $K^* = \frac{\sigma_i}{\sigma_{comp}}$ is the normalized stress intensity; $\sigma_i = \sqrt{3I_2(D_\sigma)}$ is stress intensity, Pa; $I_2(D_\sigma)$ is the second invariant of the stress tensor deviator D_σ, Pa^2; σ_{comp} is the uniaxial compressive strength of rock, Pa. The established correspondence in the form of a ratio (2) is fundamental for calculating the degree of loading on rib pillars, as it reflects the stress state of these pillars, which is caused by a variety of geological and geotechnical conditions in the room-and-pillar mining system. So, using mathematical modelling methods based on equation (2), the estimates were obtained for changes in the bearing capacity of rib pillars, taking into account destruction of the technological interlayer [10], as well as changes in loading of pillars over time [11].

In order to simplify the procedure for assessing the degree of loading of rib pillars, including mining conditions uncovered by the Turner–Shevyakov method, a new relationship was proposed based on the results of mathematical modeling in [12]. This relationship establishes a linear correlation between the normalized value of stress intensity determined at the central point of a pillar and the degree of load calculated using the Turner–Shevyakov method:

$$C \approx 1.05 \cdot K_c^* - 0.1, \quad (3)$$

where K_c^* — is the normalized stress intensity determined at the central point of the pillar. Relation (3), in particular, is used to analyze the loading degree of a pillar during mining of two productive layers with coaxial and non-coaxial arrangement of chambers [12].

Another factor influencing the bearing capacity of rib pillars is jointing in the peripheral parts of the pillars, caused by the redistribution of rock pressure during excavation of adjacent chambers. Jointing causes delamination and exfoliation of rocks in the marginal part of the pillar, up to its collapse. From the point of view of the rib pillar mechanical behavior, the presence of discontinuity zones in the marginal part leads to a local decrease in mechanical properties and to the change in the stress–strain behavior of the entire pillar. As a confirming example, **Figure 1** shows the measurement results of the deformation modulus across the width of rib pillar No. 2 in Block I of the Gremyachaya potassium salt mine [13]. The measurements were carried out using a hydraulic jack with a step of 0.3 meters according to the method described in work [14].

It can be seen from the figure that in the marginal zones of the pillar, there is a decrease in the deformation modulus by 15–20%, caused by the presence of jointed rock zones. The size of these zones is 0.6 m, which is 26% of the width of the pillar. It follows from the given example that the presented factor cannot be classified as insignificant and its consideration when assessing the bearing capacity of rib pillars is an urgent task.

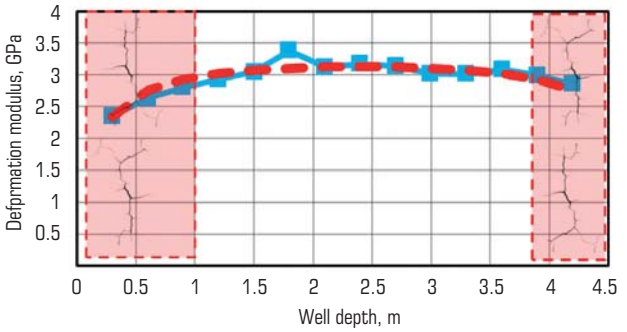

Fig. 1. Deformation modulus in rib pillar No. 2 [13] (red line—average value)

This article is devoted to the study of the influence exerted by a decrease in mechanical properties on the stress–strain behavior and on the bearing capacity of a rib pillar, with its various proportions (pillar shape factor), in case of the varying effective pressure.

Inclusion of elastic moduli reduction in assessment of bearing capacity of rib pillars

Relationship (3), which determines the loading degree of the rib pillar, operates only with force characteristics (stress and uniaxial compression strength), which are actually insensitive to changes in the mechanical properties of the pillar rock. This approaches proposes an approach that takes into account:

- The reduction of the uniaxial compression strength σ_{comp} with a decrease in elastic moduli and
- the nature of deformation state of the rib pillar.

In order to study the effect of a decrease in elastic moduli on the uniaxial compression strength σ_{comp}, we reviewed the Russian and foreign scientific literature devoted to the construction of phenomenological relationships between the ultimate strength and Young's modulus of rock. **Table** presents expressions for different types of rocks. It is evident that dependencies have both linear and exponential forms.

The choice of a suitable relation for VKSD was based on the assumption that the same dependences apply to the tangential deformation modulus D^y. A comparison was made between the predicted values of the compression strength σ_{comp} or the tangential deformation modulus D^y with the properties of sylvinite from productive stratum Kr II, which are rated in regulatory documents: $\sigma_{comp}^0 = 23$ MPa and $D_0^y = 1.1$ GPa.

The most suitable phenomenological relationship was found to be expression (7), which was obtained during testing of dolomites. According to it, the relative error of the uniaxial compression strength assessment in VKSD sylvinite does not exceed 12%. In the subsequent numerical modeling, in order to take into account the decrease in the compression strength with a decrease in the tangential deformation modulus, relation (7) was corrected with respect to the error of the initial (regulatory) values:

Phenomenological relationships between compression strength and Young's modulus of rock

N	Phenomenological relationship	$E / E_0 \cdot (\sigma_{comp} / \sigma_{comp}^0)$	Rock type
1	$E = (226\sigma_{comp} + 1.22 \cdot 10^5)98066.5$	15.6	sandstone [15]
2	$E = 455\sigma_{comp}$	9.51	iron ore [16]
3	$E = (395\sigma_{comp} + 0.044 \cdot 10^5)98066.5$	8.3	coal [17]
4	$\sigma_{comp} = 2.28 + 4.1089\,E$	1.18	sandstone [18]
5	$\sigma_{comp} = 7.97\,E^{0.91}$	0.37	shale [18]
6	$\sigma_{comp} = 13.8\,E^{0.51}$	0.63	limestone [18]
7	$\sigma_{comp} = 25.1\,E^{0.34}$	1.12	dolomite [18]
8	$\sigma_{comp} = \frac{122.11E}{39.37+E}$	0.14	limestone [19]
9	$\sigma_{comp} = 0.0084\,E$	0.4	sandstone [20]

$$\sigma_{comp}\left(D^{y}\right)=25.1D^{y0.34}-0.12\sigma^{0}_{comp}, \quad (4)$$

where σ_{comp} is the current uniaxial compressive strength at the tangential deformation modulus D^{y}; $\sigma^{0}_{comp}=23$ MPa is the standard value of the compression strength for VKSD sylvinite.

We modify the (3) to take into account the nature of deformation state of the rib pillar, supplementing it with the normalized deformation intensity:

$$C_{\sigma\varepsilon}=1.05\left(\frac{\sigma_i\left(D^{y}_{0}\right)}{\sigma_{comp}}\frac{\varepsilon_i\left(D^{y}_{0}\right)}{\varepsilon_{comp}}\right)^{\frac{1}{2}}-0.1, \quad (5)$$

where $\varepsilon_i=\sqrt{I_2\left(D_\varepsilon\right)}$ is the strain intensity; $I_2\left(D_\sigma\right)$ is the second invariant of the stain tensor deviator D_ε; ε_{comp} is the limit compression strain determined from the equality $C_{\sigma\varepsilon}=C$ of the loading degrees calculated for an undamaged pillar. The advantage of relation (5) is that, when determining the loading degree of a pillar, it considers both the intensity of stresses and the intensity of strain at its center.

The final relation for the degree of rib pillar loading C_{all}, taking into account the decrease in aggregate strength of rock with the decrease in the tangential deformation modulus and the nature of the pillar deformation, with regard to (4) and (5), is given by:

$$\begin{cases} C_{all}=1.05\left(\dfrac{\sigma_i\left(D^{y}\right)\varepsilon_i\left(D^{y}\right)}{\sigma_{comp}\left(D^{y}\right)\varepsilon_{comp}\left(D^{y}\right)}\right)^{\frac{1}{2}}-0.1 \\ \sigma_{comp}\left(D^{y}\right)=25.1D^{y0.34}-0.12\sigma^{0}_{comp} \\ \varepsilon_{comp}\left(D^{y}\right)=\sigma_{comp}\left(D^{y}\right)\dfrac{\varepsilon_i\left(D^{y}_{0}\right)}{\sigma_i\left(D^{y}_{0}\right)} \end{cases}, \quad (6)$$

where D^{y} is the effective tangential deformation modulus of a pillar; $\sigma_{comp}(D^{y})$, $\varepsilon_{comp}(D^{y})$ are the current compression strength and compression strain dependent on the effective deformation modulus; $\dfrac{\varepsilon_i\left(D^{y}_{0}\right)}{\sigma_i\left(D^{y}_{0}\right)}$ is the ratio of the strain and stress intensity at the central point of an intact pillar, calculated for a given geometry and loading conditions. The use of relation (6) to calculate the loading degree of pillars in specific mining and geological conditions requires determining the dependence of the tangential deformation modulus reduction on the magnitude of the effective rock pressure.

Experimental dependence of elastic moduli on maximum applied stress in sylvinite

To correlate the elastic properties of sylvinite and the level of stress, including the stage of crack initiation, a series of tests were conducted on sylvinite subjected to cyclic uniaxial compression. A batch of cubic sylvinite samples made from rocks of productive strata Kr II consisted of five specimens with an edge size of 20 ± 2 mm. The non-parallelism of the edges dID not exceed 40 μm. The selected sample size relates to the possibility of studying the evolution of their internal structure using X-ray computed tomography during successive sample loading cycles. The description of the research results is outside the scope of this article. The tests were carried out on a Zwick Z250 electromechanical press in the stiff loading mode with a crosshead movement speed of 0.05 mm/min. The experiments were carried out until complete destruction, i.e. loss of the load-bearing capacity of the samples. The number of cycles before failure ranged from 6 to 9 from sample to sample. Based on the results of the compression experiment, the tangential deformation modulus D^{y} of sylvinite was determined in each cycle using the method from [21]. Before determining the tangential deformation modulus, the stress–strain curve was adjusted for the stiffness of the testing machine.

Due to the variability in the elastic properties of sylvinite samples, caused by different mineral compositions and by the presence of clay materials, the dependences of the normalized tangential deformation modulus D^{y} on the maximum applied stress in a cycle were constructed. The modulus determined for each loading–unloading cycle was normalized to the value of the tangential deformation D^{y}_{0} determined in the first cycle for each sample. The general dependence of the normalized tangential deformation modulus D^{y}/D^{y}_{0} on the maximum applied stress in a cycle is illustrated in **Fig. 2*a***. It is clear from the figure that the generalized experimental dependence of the tangential deformation modulus of sylvinite on the maximum applied stress in each cycle shows a little variation between samples within each cycle, and can be described using a single analytical function. Based on the experimental dependence, an approximation was constructed taking into account that the normalized tangential deformation modulus D^{y}/D^{y}_{0} is equal to one at zero level of the applied stress, and is equal to zero at the value of the applied stress corresponding to the regulatory compression strength $\sigma^{0}_{comp}=23$MPa:

$$\frac{D^{y}}{D^{y}_{0}}=f_1\left(\sigma_{\max}\right)=2.33-0.83\cosh\left(0.07\left(0.74\sigma_{\max}-13.17\right)\right)-$$
$$-0.83\sinh\left(0.07\left(2.4+0.74\sigma_{max}\right)\right), \quad (7)$$

where $\sigma_{\max}$ is the maximum axial stress in a cycle. The graphical representation of constructed approximation function (7) is shown in **Fig. 2*b***.

In [22–24], the experimental study of changes in the elastic properties of rocks under different types of loading shows that the accumulation of damage (microcracks) leads not only to a decrease in the elastic modulus but also to an increase in Poisson's ratio. Following continuum mechanics of damage, the correction for Poisson's ratio can be found from the condition of constancy of the first Lame parameter with regard to (7):

$$\frac{\nu}{\nu_0}=f_2\left(\sigma_{\max}\right)=\frac{1}{4\nu_0^2}\left(f_1\left(\sigma_{\max}\right)\eta-\nu_0+\sqrt{8\nu_0^2+\left(\nu_0-f_1\left(\sigma_{\max}\right)\eta\right)^2}\right), \quad (8)$$

where $\eta=\left(2\nu_0^2+\nu_0-1\right)$; ν_0 is initial (regulatory) Poisson's ratio of sylvinite. The graphical representation of constructed approximation function (8) is shown in **Fig. 2b**.

Thus, as a result of a series of experiments on cyclic uniaxial compression of sylvinite cubes, the approximations of the dependences of the elastic moduli (tangential deformation modulus and Poisson's ratio) on the maximum applied stress in a cycle were obtained.

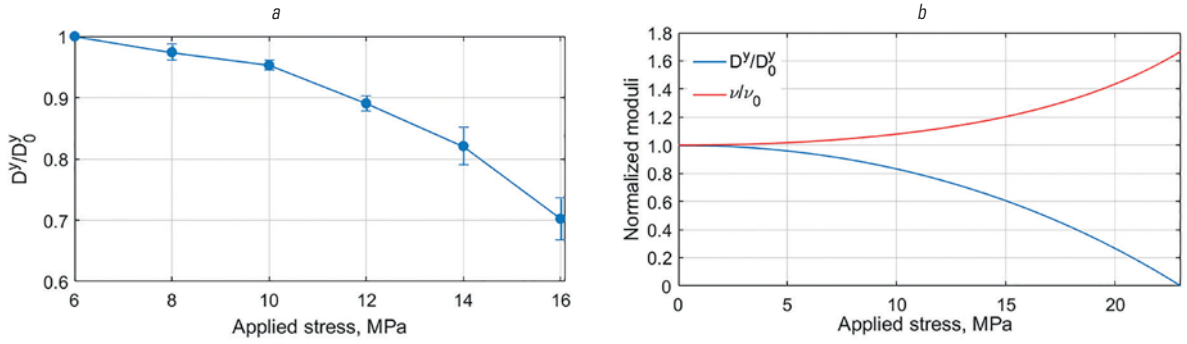

Fig. 2. Experimental dependence of normalized tangential deformation modulus D^{y}/D^{y}_{0} of red sylvinite on maximum applied stress per cycle (*a*) and approximations of normalized elastic moduli based on it (*b*)

Numerical stress–strain modeling of pillar with regard to changes in elastic moduli

Problem formulation

The assessment of the effect of sylvinite jointing on the level of pillar loading was based on the mathematical stress–strain modeling of the pillar at various parameters of the model. The basic calculation scheme is shown in **Fig. 3**. The mathematical modeling was carried out in plane deformation state. We consider a pillar between two chambers cut by Ural-20R shearer and having a fixed size: mineable height $m_0 = 5$ m, the width $a = 5.1$ m. The depth to the roof of the chambers is $H_0 = 363$ m. The width of the pillar was varied as 3.75, 5, 7.5 and 10 m, which corresponded to the pillar shape factors λ (the ratio of width to height) of 0.75, 1, 1.5 and 2.

At the upper boundary of the calculation domain and at the boundaries of the chambers, the condition of stress-free was set, while at the lateral and lower boundaries of the massif, no displacements were allowed normal to the boundaries. The entire computational domain is subjected to gravitational stresses. The effective pressure on the pillar in the calculations varied in the range from $P_1 = \gamma H_0$ (the pressure of the overlying rock mass in case of only two chambers) to $\gamma H_0 \frac{a+b}{b}$ (the condition of complete undermining), where γ is the bulk density of rock, *b* is the width of the pillar and *a* is width of a chamber.

The numerical stress–strain modeling of the rib pillar was carried out using the finite element method in the commercial COMSOL Multiphysics package. The calculation domain was divided into triangular finite elements with condensation towards the pillar, at a minimum finite element size of b/1200. The following values of material parameters were adopted for the calculations:

- sylvinite density $\rho = 2200$ m^3/kg;
- the tangential deformation modulus is a function of the maximum principal stress σ_1, $D^y = f_1(\sigma_1)\ D_0^y$, when $D_0^y = 1.1$ GPa, a function $f_1(\sigma_1)$ is determined by relation (7);
- Poisson's ratio is given by the dependence $\nu = f_2(\sigma_1)\nu_0$, when $\nu_0 = 0.3$, a function $f_2(\sigma_1)$ is determined by relation (8).

Modeling results

Figure 4*a* shows the dependence of the effective tangential modulus of deformation at the central point of the pillar (point A1) on the value of the effective pressure in relative units. The dependencies show how the tangential deformation modulus at the point A1 decreases at a given level of the effective pressure and for a given pillar geometry, relative to the initial (regulatory) value D_0^y. It is clear from the figure that the greatest change in the tangential deformation modulus occurs for the narrowest pillar (λ = 0.75) and under conditions of complete undermining. The value of this change is 22.4%. For wide pillars (λ>1), the relative change in the tangential modulus does not exceed 6%. Similar dependencies are constructed for effective Poisson's ratio (**Fig. 4*b***). The maximum change in Poisson's ratio is 10.5% and occurs for the narrowest pillar at the maximum effective pressure. For wide pillars, the change in Poisson's ratio does not exceed 3%. Thus, the obtained results allow concluding that the change in the elastic moduli caused by jointing of salt rocks is insignificant in the case of pillars with a shape factor λ > 1.

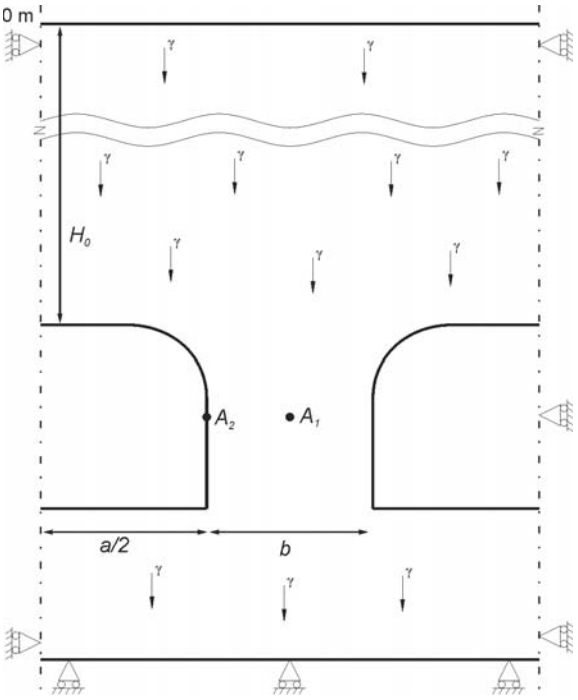

Fig. 3. Basic calculation scheme

Figure 5 shows the dependence of the horizontal convergence in a chamber (horizontal displacement of the central point A2, see Fig. 3) on the effective pressure for various pillar sizes. The relative values of convergence (Fig. 5*b*) determine how much the displacement of the side wall is greater when taking into account the change in elastic modulus than when elastic properties are constant. It can be seen from the figure that, despite the horizontal convergence from 15 to 22 cm depending on the pillar width (Fig. 5*a*), the difference from the calculation with the regulatory properties varies between 2 and 7.5 cm (Fig. 5*b*). The correction to the horizontal convergence of the pillar, taking into account jointing of rock in relation to the original width of the pillar, varies within the range from 0.02% to 0.2%.

Relations (6) and the results of multiparameter numerical modeling of the stress–strain behavior of the pillar were used to calculate the loading degree of the pillar with regard to jointing of salt rocks (the dependence of the elastic and strength properties on the current maximum principal stress). First, for the central point A1 in the pillar, the effective compression strength σ_{comp} is calculated (relation (6.2)), based on the effective tangential

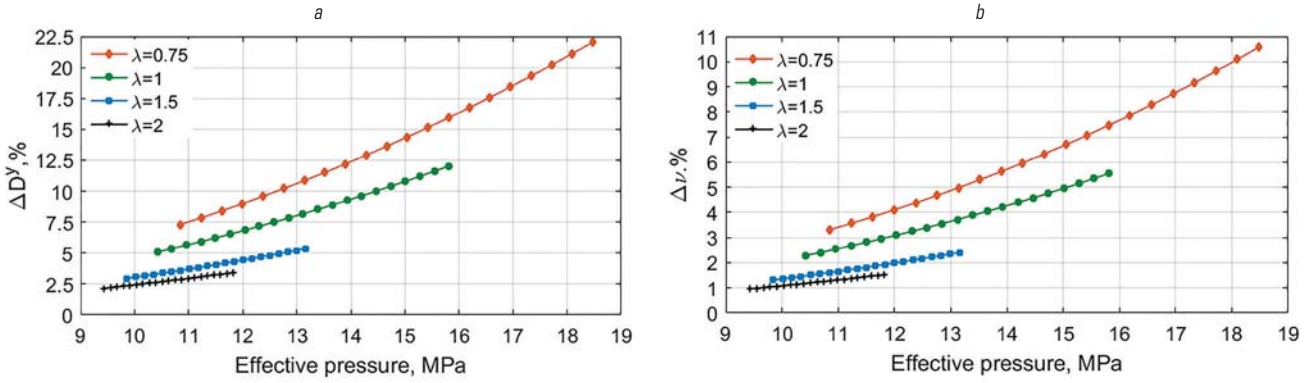

Fig. 4. Effective tangential deformation modulus (*a*) and Poisson's ratio (*b*) at the pillar center as function of effective pressure for various pillar shape factors

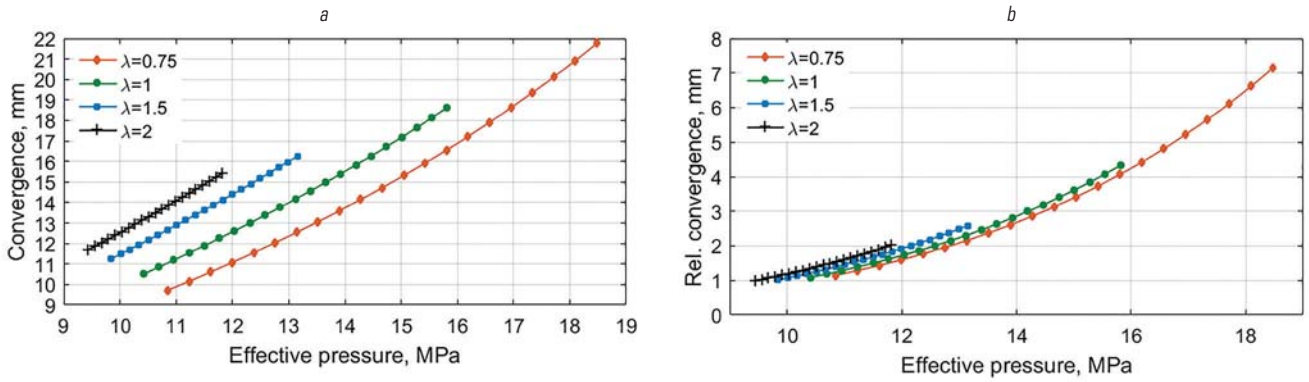

Fig. 5. Horizontal convergence of pillar versus effective pressure for different shape factors (absolute values (*a*), relative change (*b*))

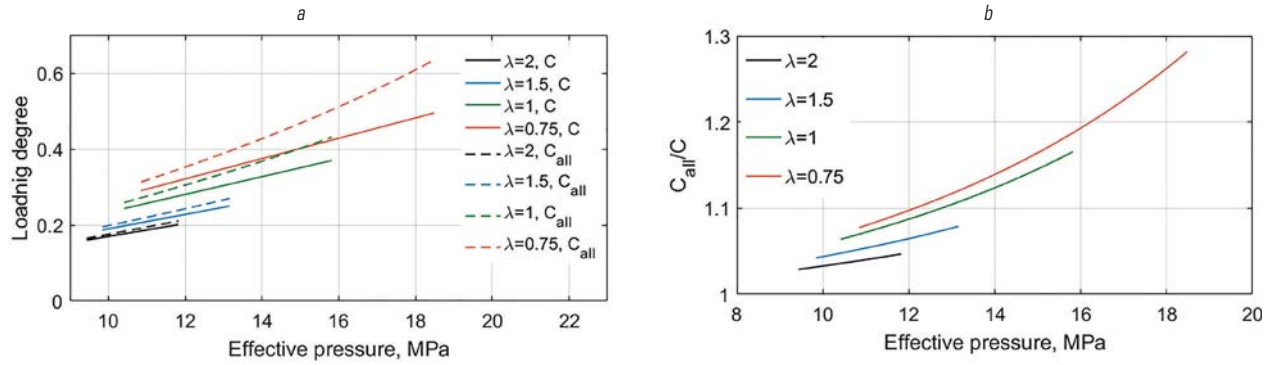

Fig. 6. Pillar loading degree C_{all} (relation (6)) and C (relation (3)) (*a*) and their ratio C_{all}/C (*b*) versus effective pressure calculated for different shape factors λ

deformation modulus D^y and on the standard uniaxial compression strength value $\sigma^0_{comp} = 23$ MPa. Next, based on the results of the elastic calculation (with constant elastic moduli) and the effective compression strength, the compression strain $\varepsilon_{comp}(D^y)$ is calculated (equation (6.3)). As a result, the limit values of σ_{comp} and ε_{comp} for the given pillar width and effective pressure are used to calculate the loading degree on the rib pillar, C_{all} (equation (6.1)).

Figure 6 shows the obtained dependencies of the pillar loading degree with a without regard to sat rock jointing, C_{all} and (C), respectively, on the effective pressure for different shape factors λ of the pillars.

The rib pillars with a shape factor greater than one are characterized by small changes in the loading degree even under conditions of complete undermining, both without regard to cracks in rocks (sollD lines in **Fig. 6*a***) and with regard to them (dashed lines in **Fig. 6*b***). The magnitude of the loading degree C_{all} at λ=2 and λ=1.5 is greater than the loading degree C by no more than 4.8% and 8%, respectively (Fig. 6*b*).

The situation is different for λ ≤ 1. In the case of rib pillars with square cross-sections (λ = 1), the estimated loading degree differs by 16.5% based on relations (6) and (3). Inclusion of jointing of salt rocks in the calculation leads to an increase in the loading degree of the pillar from 0.36 to 0.41 (Fig. 6*a*) for the conditions of complete undermining (maximum effective pressure). For narrow pillars (λ=0.75), the difference between the values of C_{all} and C varies from 8% at the minimum to 28% at the maximum effective pressure. In this case, under conditions of complete undermining, the loading degree of a narrow pillar ranges from 0.5 (without regard to salt rock jointing) to 0.63 (with regard to salt rock jointing).

Conclusions

The article proposes a modification to the calculation of the loading degree of rib pillars taking into account salt rocks jointing caused by partial unloading of rock mass during excavation of the stope. It is assumed that the presence of weakened zones in the perimeter of the pillar leads to a decrease in its bearing capacity.

The modified ratio of the loading degree of pillars takes into account the following parameters: intensity of stresses and strains, uniaxial compression strength and compression strain of rocks. Each of these parameters depends on the effective elastic moduli of salt rock. The reduction of these, in turn, depends on the magnitude of the maximum principal stress. To establish the dependence of elastic moduli on the maximum applied stress, a series of experiments were carried out on cyclic uniaxial compression of cubic sylvinite samples. It is shown that the change in the normalized tangential deformation modulus for all tested samples, with an increase in the maximum applied stress from cycle to cycle, can be approximated by a single curve. As a result of the analysis, an approximation to this dependence by a linear combination of hyperbolic functions was proposed. From the condition of the constancy of the first Lame parameter, the dependence was found for normalized Poisson's ratio of sylvinite on the value of the maximum applied stress.

In order to determine the phenomenological dependence of the uniaxial compression strength sylvinite on its Young's modulus, the review of the Russian and foreign literature was conducted. As a result, based on the regulatory values of Young's modulus and the uniaxial compression strength, the correlation was selected that satisfies VKSD sylvinite. It should be noted that a separate task is to clarify this phenomenological dependence based on the analysis of the existing database on the elastic and strength properties of VKSD salt rocks.

The modified equation for calculating the loading degree of rib pillars was tested using the results of mathematical stress–strain modeling of rib pillars, both with and without regard to the dependence of the elastic moduli on the maximum principal stress values. The calculation scheme is designed for the conditions of productive strata Kr II. Multivariate modeling is carried out for pillars of different shapes at different levels of effective pressure.

As a result of the conducted multiparameter calculations, it is found out that taking into account the jointing has the greatest influence on the bearing capacity of pillars with a shape factor λ ≤ 1 under conditions of complete undermining. Thus, in the case of a pillar with λ=0.75, the degree of its loading will change from 0.5 (with no regard to jointing) to 0.63 (with regard to jointing). This corresponds to an increase of 26% in the loading degree. In this case, the change in the tangential modulus of deformation and Poisson's ratio at the central point of this pillar was 22.4% and 10.5%, respectively. The proposed ratio for determining the loading degree of a rib pillar, considering the decrease

in aggregate rock strength with a decrease in the elastic moduli and the nature of its deformation, can be used to develop a method for assessing the current bearing capacity based on instrumental measurements of elastic modulus profiles along the thickness of the pillar.

Acknowledgment

The work was carried out as part of a major scientific project supported by the Ministry of Science and Higher Education of the Russian Federation, Agreement No. 075-15-2024-535 dated 23 April 2024.

References

1. Golasowski J., Vochta R., Hudeček V., Mikoláš M., Dvořák P. Room and pillar mining at OKD, as in the Czech Republic. *14th International Multidisciplinary Scientific Geoconference & Expo SGEM 2014*. Albena, Bulgaria, 2014. pp. 529–536.
2. Jong-Gwan Kim, Mahrous A. M. Ali, Hyung-Sik Yang. Robust design of pillar arrangement for safe room-and-pillar mining method. *Geotechnical and Geological Engineering*. 2019. Vol. 37. pp. 1931–1942.
3. Permyakov R. S., Romanov V. S., Beldy M. P. Salt Mining Technology. Moscow : Nedra, 1981. 271 p.
4. Makarov A. B., Rasskazov I. Y., Saksin B. G., Livinsky I. S., Potapchuk M. I. Geomechanical evaluation of roof-and-pillar parameters in transition to underground mining. *Journal of Mining Science*. 2016. Vol. 52, No. 3. pp. 438–447.
5. Instructions (Measures) for the Protection of Uralkali Mines from Flooding and Protection of Objects on the Earth's Surface from Harmful Effects of Underground Mining at Verkhnekamskoe Salt Deposit (Appendix 1). Perm : Berezniki, 2022. 117 p.
6. Instructions (Measures) for the Protection of EuroChem-UKK LLC's Mine from Flooding and Protection of Objects on the Earth's Surface from Harmful Effects of Underground Mining at Verkhnekamskoe Salt Deposit During Development of Sylvinite Formations. Perm : Berezniki, 2025. 114 p.
7. Tournaire M. Dimensions to be given to the pillars of the carriers and the Pressures to which the terrains are subjected in the depths. *Annales des mine*. 1884. Vol. 5. pp. 415–429.
8. Shevyakov L. D. Calculation of strength and strains of safety pillars. *Izvestiya AN SSSR. Otdelenie tekhnicheskikh nauk*. 1941. No. 7-9.
9. Baryakh A. A., Samodelkina N. A. To the calculation of pillar stability under condition of chamber mining. *Journal of Mining Science*. 2007. Vol. 43, No. 1. pp. 8–16.
10. Baryakh A. A., Lobanov S. Y., Shumihina A. Y., Lomakin I. S. Analysis of changes in load-carrying ability of rib pillars during the failure of technological parting. *MIAB*. 2013. No. 1. pp. 27–33.
11. Baryakh A. A., Lobanov S. Y., Lomakin I. S. Analysis of time-to-time variation of load on rib pillars in mines of the Upper Kama Potash Salt Deposit. *Journal of Mining Science*. 2015. Vol. 51, No. 4. pp. 696–706.
12. Baryakh A. A., Lomakin I. S., Samodelkina N. A., Tenison L. O. Loading of rib pillars in multiple seam mining at the Upper Kama salt deposit. *MIAB*. 2023. No. 1. pp. 5–19.
13. Pospelov D. A., Pankov I. L., Toksarov V. N., Naparina D. V. Studying deformation properties of salt rocks in laboratory and in-situ environments *Izvestija Tulskogo Gosudarstvennogo Universiteta. Nauki o Zemle*. 2024. No. 4. pp. 700–713.
14. Pospelov D. A., Toksarov V. N., Beltyukov N. L. Methodology for assessing the deformation modulus of rocks in a marginal massif using a borehole hydraulic jack. *Gornoye ekho*. 2022. No. 1(86). pp. 51–57.
15. Matveev B. V., Mikheeva M. M., Kartashov Yu. M. et al. Catalogue of Strength And Deformability Indices of Rock Samples arom Coal Deposits. Leningrad : VNIMI Publishing House, 1973. 40 p.
16. Tokhtuev G. V., Borisenko V. G., Titlyanov A. A. Physical and Mechanical Properties of Rocks of Krivbass. Kyiv : Gosgortekhizdat of the Ukrainian SSR, 1962. 102 p.
17. Altayev Sh. A., Smirnov L. N. On some physical and mechanical properties of rocks of the Karaganda coal basin (Saransk section). *Nauchnie Trudy Karagandinskogo nauchno-issledovatelskogo ugolnogo instituta*. 1966. Vol. 21. pp. 280–289.
18. Chang C., Zoback M. D., Khaksar A. Empirical relations between rock strength and physical properties in sedimentary rocks. *Journal of Petroleum Science and Engineering*. 2006. Vol. 51, Iss. 3-4. pp. 223–237
19. Moradian Z. A., Behnia M. Predicting the uniaxial compressive strength and static Young's modulus of intact sedimentary rocks using the ultrasonic test. *International Journal of Geomechanics*. 2009. Vol. 9, No. 1. pp. 14–19.
20. Malik M. H., RashID S. Correlation of some engineering geological properties of the Murree formation at lower Topa (Murree district), Pakistan. *Geological Bulletin University OF Peshawar*. 1997. Vol. 30. pp. 69–81.
21. Baryakh A. A., Asanov V. A., Pankov I. L. Physical and Mechanical Properties of Salt Rocks of the Verkhnekamskoye Potash Deposit: Textbook. Manual. Perm: Publishing house of Perm State Technical University, 2008. 199 p.
22. Stavrogin A. N., Protosenya A. G. Mechanics of Deformation and Destruction of Rocks. Moscow : Nedra, 1992. 224 p.
23. Martin C. D., Chandler N. A. The progressive fracture of Lac du Bonnet granite. *International Journal of Rock Mechanics and Mining Sciences & Geomechanics Abstracts*. 1994. Vol. 31, Iss. 6. pp. 643–659.
24. Eberhardt E., Stead D., Stimpson B. Quantifying progressive pre-peak brittle fracture damage in rock during uniaxial compression. *International Journal of Rock Mechanics and Mining Sciences*. 1999. Vol. 36. pp. 361–380. EM

M. RADOVANOVIC[1], *Teaching Assistant, MSc in Mining Engineering, PhD Candidate, mlradovanovic@tfbor.bg.ac.rs*
R. PANTOVIC[1], *Head of the Rock mechanics laboratory, Professor*
D. PETROVIC[1], *Head of the Underground mining department, Professor*
M. STAJIC[1], *Teaching Assistant, MSc in Mining Engineering, PhD Candidate*

[1]*University of Belgrade, Technical faculty in Bor, Bor, Republic of Serbia*

DETERMINATION OF THE EXCAVATION BLOCK BOTTOM STRUCTURE PARAMETERS USING FINITE ELEMENT NUMERICAL METHOD STABILITY ANALYSIS

Introduction

In the most of ore deposits at shallower depths, with high grade ores, the exploitation has been completed or is in the final phase, so the main characteristic of underground exploitation all over the world is the increasing of excavation depth with lower grades ore. Increasing of exploitation depth is accompanied by deterioration in the operating conditions: a change in the physical and mechanical properties of rocks, an increase in the temperature of geological environment, steady rock pressure rise in workings and its manifestation [1]. Even in such conditions, achieving a positive economic result in order to enable the profitability exploitation, are being strived. Making a profit with the lowest possible production costs is one of the primary goals of exploitation [2]. This is the reason why there is an inevitable need to reduce the costs of exploitation and obtaining ore by investing in the development of new technologies, modernization of infrastructure, optimization and better organization of production

The future of underground exploitation is reflected in the increase of the depth at which it takes place, considering that deposits at lower depths are mostly exploited. The increase in depth represents a challenge in mine design, because the increase in depth is accompanied by more difficult mining conditions. Also, one of the characteristics of underground exploitation in past years is the constant reduction of ore grades. That is the reason why caving methods take an important place in present mining. To provide safety mining environment using caving methods at greater depths it is necessary to ensure the stability of the excavation blocks. This can be achieved by selecting the optimal parameters of the excavation blocks and the proper construction of the bottom structure of the excavation blocks. In this paper, an analysis of the stability of the facilities at the bottom structure of excavation block was performed. The results of the numerical finite element analysis of the stress-strain state show that with proper bottom structure construction of the excavation block and with an appropriate layout of the loading chambers and drifts, satisfying stability can be achieved which ensures safety working conditions.

Keywords: *underground mining, mining methods, stability analysis, numerical methods, excavations, bottom structure, stresses*
DOI: *10.17580/em.2025.05.08*